Variable Optical Buffer Using Slow Light in Semiconductor Nanostructures

CONNIE J. CHANG-HASNAIN, FELLOW, IEEE, PEI-CHENG KU, STUDENT MEMBER, IEEE, JUNGHO KIM, AND SHUN-LIEN CHUANG, FELLOW, IEEE

Invited Paper

A compact variable all-optical buffer using semiconductor quantum dot (QD) structures is proposed and analyzed. The buffering effect is achieved by slowing down the optical signal using an external control light source to vary the dispersion characteristic of the medium via electromagnetically induced transparency effect. We present a theoretical investigation of the criteria for achieving slow light in semiconductor QDs. A QD structure with presence of strain is analyzed with the inclusion of the polarization-dependent intersubband dipole selection rules. Experimental methods to synthesize and the measurements of coherent properties in state-of-the-art QDs are surveyed. Slow-light effects in uniform and nonuniform QDs are compared. Finally, optical signal propagation through the semiconductor optical buffer is presented to demonstrate the feasibility for practical applications.

Keywords*—*Integrated optics, nanotechnology, optical buffer, quantum optics.

I. INTRODUCTION

A controllable variable optical memory is one of the most critically sought after components in optical communications and signal processing. In such a buffer, optical data would be kept in optical format throughout the storage time without being converted into electronic format. The buffer must be able to turn on to store and off to release optical data at a very rapid rate by an external command. This seemingly simple function to this date has never been realized, in spite of much previous research.

Manuscript received December 22, 2002; revised June 25, 2003. This work was supported by the National Science Foundation under Award ECS-0123512 and by the Defense Advanced Research Projects Agency (DARPA) under CSOM Award F30602-02-2-0096.

C. J. Chang-Hasnain and P.-C. Ku are with the Department of Electrical Engineering and Computer Science, University of California at Berkeley, Berkeley, CA 94720 USA (e-mail: cch@eecs.berkeley.edu; cch@photonics.eecs.berkeley.edu; peicheng@eecs.berkeley.edu).

J. Kim and S.-L. Chuang are with the Department of Electrical and Computer Engineering, University of Illinois at Urbana-Champaign, Urbana, IL 61801 USA (e-mail: jkim47@uiuc.edu; s-chuang@uiuc.edu).

Digital Object Identifier 10.1109/JPROC.2003.818335

Recently, we proposed a novel approach of making an all-optical buffer in semiconductors [1]–[3]. Our basic idea centers on making a medium that can controllably slow down optical transmission such that it is effectively an optical memory. By controlling the group velocity reduction factor, the memory storage time can be adjusted to desired values. Our approach involves engineering the material dispersion curve (i.e., refractive index as a function of frequency) with the use of semiconductor quantum dots (QDs) under a mechanism called the electromagnetically induced transparency (EIT).

There have been major breakthroughs recently in achieving slow or stopped light in atomic gases and solid-state material using EIT [4]–[8]. Slowdown factors as high as seven orders of magnitude have been demonstrated. The slowing principle is based on creating interference between the electronic states of the atomic vapor by means of a pump optical field, which thus modifies the real and imaginary parts of the refractive index of the medium. The resulting effect is a greatly reduced group velocity and optical absorption for the signal.

Historically, semiconductor-based devices have proven to create far more importance compared with gas- or solid-state-based ones. There are plenty of historical examples: semiconductor transistors versus vacuum tubes, and diode lasers versus gas lasers, etc. The vast potential advantages include compactness, low power consumption, and opportunity for monolithic integration.

Semiconductor QDs are artificial semiconductor crystallites that are small enough such that the electrons are confined in three dimensions resulting in discrete energy states, governed by quantum mechanics. Many describe QDs as gigantic "man-made" atoms (typically consisting of 10 000 or more atoms). The discrete energy states make QDs an excellent candidate for slowing down light. One important question is whether semiconductor QDs have the required characteristics for slow light. In particular, one of the concerns

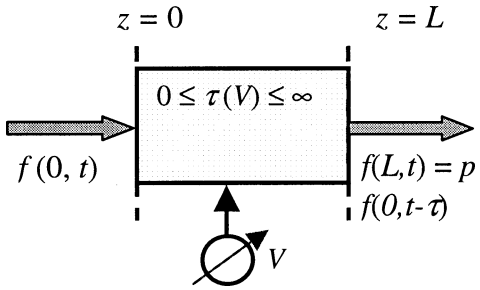

Fig. 1. Definition of an all-optical buffer.

is the single-dot homogeneous linewidth, which is many orders of magnitude broader than that of atomic gases. In addition, experimentally the state-of-the-art QD sizes are still rather nonuniform. In this paper, we present our modeling effort and address these two issues. Our calculations show that semiconductor QDs are promising to achieve a level of slowdown (on the order of 100) that is reasonably useful for optical switching applications.

This paper is organized as follows. First, we define the term optical buffer, followed by a review of various potential applications, previous approaches, the progress of EIT, and the state-of-the-art QD properties. We will discuss our model and calculations to address the criteria of semiconductor QDs for attaining the slow-light effect, particularly on homogeneous and inhomogeneous linewidths, and discuss the feasibility to achieve slow light. Device structures are also proposed.

A. Definition of Optical Buffers

There has been no published definition for an all-optical buffer. In this paper, we adopt the following definition, primarily from common sense. An all-optical buffer has its input and output data streams in optical format without optical-electrical-optical (OEO) conversion. The buffer would store the optical signal for a certain amount of time τ with limited amount of distortion or impairment. Further, the turn-on or turn-off should be variable with an external control. We emphasize that only the data stream needs to be all-optical; the header, on the other hand, can have OEO conversion and processed. This is very much in line with what is being used for all-optical cross connect and all-optical networks.

Schematically, an optical buffer can be represented by Fig. 1. The output data stream $f(L,t)$ is essentially a copy of the input data $f(0,t)$; it is equal to the multiple of a proportionality constant p with a time delay τ that is variably controlled by an external source V. L is the length of the device. It is important that signal distortion and dispersion must be within a certain tolerable range to result in a minimum level of impairment. The requirements for other parameters, such as turn-on and turn-off times and optical loss, may vary depending on applications.

B. Potential Applications

The most influential application that optical buffers could enable is perhaps all-optical routers in packet-switched networks. There have been rapid advances in optical fiber communications in the past two decades. With the advent of erbium-doped fiber amplifiers and wavelength-division-multiplexed systems, transmission capacity as high as 10 Tb/s through a single fiber has been demonstrated in laboratories. This huge capacity can create serious data traffic congestions at major interconnections. Electronic routers at subterabits/second rate exist today. The scalability to a higher throughput is very difficult. Furthermore, the electric power and space demanded by such a router makes the electronic routers highly undesirable. An all-optical packet-switched network can potentially eliminate this major bottleneck.

A router is used in networks (such as the Internet) to interconnect end-user systems to each other where packets are the basic units of information that are transported. A router often connects many networks and performs decisions on how to send packets from its source to its destination in the network. Packet switching is a method of communication whereby information is broken up into blocks of limited length called packets. They are then switched in a network by routers. The blocks can be fixed-length or variable-length but limited. A packet also contains a header, which describes the address of the source and destination for the data. The Internet is a packet-switched network; thus, data (in the form of e-mail, a web page, image, news message, etc.) are sent as packets of various lengths and allow many users to share the same data path. In today's network, data are transmitted in optical format and routed and switched in electronic format.

The key building blocks of an electronic router include a switch fabric, processors, and buffers. Given that all-optical switches and signal processing have been demonstrated previously [9], the key missing component for an all-optical router is an all-optical buffer.

Fig. 2 is a schematic showing the function of an optical buffer to resolve contention in an optical switch. With optical buffers, one packet can be stored in the buffer temporarily, allowing the other packet to go first. Until the traffic is cleared at the output port, the packet stored in the buffer is released. An all-optical router can potentially alleviate the traffic congestion in future very-high-bandwidth networks.

In addition to the application in optical communication systems, an optical buffer can enable several other possible applications including optical signal processing, radio frequency (RF) photonics such as phased-array antennas, nonlinear optics by increasing the effective interaction length, and time-resolved spectroscopy.

As an example, one of the most elementary operations in analog signal processing is correlation

$$\int f_1(\tau) f_2(t-\tau) \mathrm{d}\tau = F_1(\omega) F_2(\omega). \tag{1}$$

The time delay τ in the integral can be implemented by an optical buffer.

Another example would be z transform in digital signal processing, defined as

$$B(z) = \sum_n b_n z^n \tag{2}$$

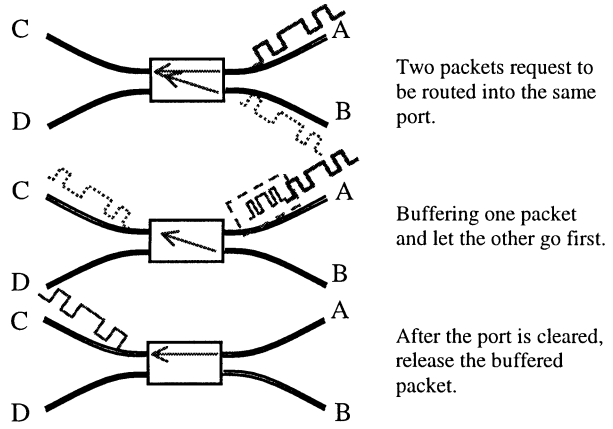

Fig. 2. Optical buffer providing contention resolution in an optical switch.

where b_n is the value of the nth bit in the digital pulse train. The operator z is a time-delay operator and can therefore be implemented by an optical buffer.

In phased-array antennas, a true-time delay instead of phase shift is required. An optical buffer can provide such functions [10], [11].

In time-resolved spectroscopy, a pump-probe configuration is often used where two short pulses with time delays relative to each other are sent into the sample. The time delay is provided by varying the optical path of the second pulse and, hence, the system is usually very bulky. A compact optical buffer can provide such time delay and makes a compact pump-probe system possible.

C. Technical Approaches

To obtain an optical buffer, in general, one must vary the medium within which the optical signal travels by either increasing the path length or reducing the signal group velocity. The former can be accomplished with the use of a fiber delay line, which will be discussed below. The latter has several possibilities. We first observe that the group velocity v_g is defined as

$$v_g = \frac{\partial \omega}{\partial k} = \frac{c - \omega \frac{\partial n(k,\omega)}{\partial k}}{n(k,\omega) + \omega \frac{\partial n(k,\omega)}{\partial \omega}} \tag{3}$$

where n is real part of the refractive index and k is the waveguide propagation constant. We can define a slowdown factor S as

$$S = \frac{c}{v_g} = \frac{n + \omega \frac{\partial n}{\partial \omega}}{1 - \frac{\omega}{c} \frac{\partial n}{\partial k}}. \tag{4}$$

From (4), we see that the group velocity can be reduced by introducing a large and positive waveguide dispersion $\partial n/\partial k$ or material dispersion $\partial n/\partial \omega$. The waveguide dispersion can be designed using gratings or periodic structure [12]. However, the most effective method is to introduce a large material dispersion using EIT, as will be discussed later. Of course, it is also possible to include both material and waveguide dispersion in one device to have an enhanced effect [3]. In the following, we will briefly review previous works.

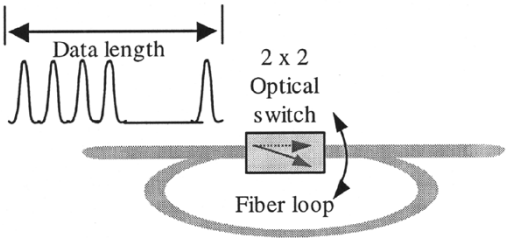

Fig. 3. Fiber delay line used as an optical buffer with fixed storage time [13].

1) Optical Fiber Delay Lines: Optical fiber delay lines have previously been referred to as an "optical buffer" [13]. One basic design typically consists of a 2×2 optical switch connected with a fiber loop (Fig. 3). Other components such as optical isolators, amplifiers, and dispersion compensation devices have also been included to reduce impairments due to reflection, loss, and dispersion.

The optical switch is first set to direct the data train into the fiber loop and subsequently is closed to allow the data to recirculate in the loop. The storage capacity, i.e., amount of data stored, is limited by the time required to travel one loop τ_{loop} subtracted by that required to set the switch. This is because when the optical data stream is longer than τ_{loop}, the data of the leading part of the packets will overlap with that in the back to cause interference. The storage time, i.e., how long the data is kept in the loop, is an integer multiple of τ_{loop}. The turn-off (release) time is also determined by τ_{loop}. This is because once a packet enters the delay line, it can only emerge at a fixed duration of time later. It is impossible to remove the packet from the delay line before that fixed time interval.

The fundamental difficulty facing this design is that the storage time is fixed or quantized by the time required to travel one loop. With the data arrival being random and unsynchronized in real networks, optical routers based on fixed delay times cannot guarantee contention-free connections throughout the network. The fixed time also makes the design of architecture very challenging. These are probably the main reasons why such buffers have not been deployed.

2) Slow Light Using Waveguide Dispersion: Studies on the light propagation in highly dispersive structures with a very slow group velocity have drawn much attention. Grating structures have been used extensively in DFB lasers and grating waveguide couplers. Recent progress on the fabrication of grating structures in fiber has opened new research areas using fiber Bragg gratings [14]. Recently, another method for achieving slowed light based on a Moiré fiber Bragg grating has been suggested [15]. A Moiré grating is formed if the refractive index variation is given by

$$n(z) = n_o + \delta n \cos\left(\frac{2\pi z}{\Lambda_S}\right) \cos\left(\frac{2\pi z}{\Lambda}\right) \tag{5}$$

where Λ is the Bragg period and Λ_S is the Moiré period. The theoretical analysis shows that the group velocity of light in the transmission band can be slowed down substantially although with a very small signal bandwidth.

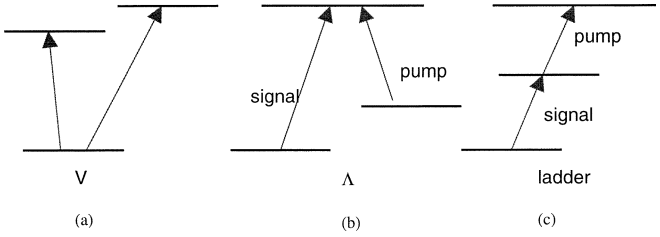

Fig. 4. Three basic schemes for three-level atoms interacting with two near-resonance electromagnetic fields: (a) ladder/cascade, (b) Λ, and (c) V schemes.

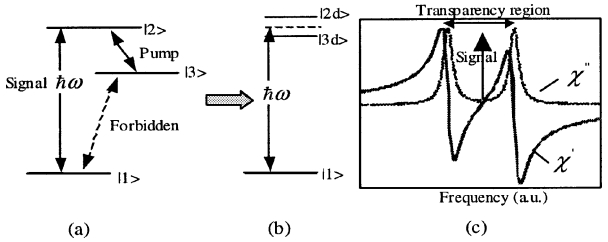

Fig. 5. (a) Λ scheme system with the pump (or coupling or control) laser in the in resonance with states $|2\rangle$ and $|3\rangle$, results in (b) a set of dressed states $|2\mathrm{d}\rangle$ and $|3\mathrm{d}\rangle$. (c) The real (χ') and imaginary (χ'') part of susceptibility for the dressed states.

Another slow-wave device configuration that is based on the sampled grating has been reported as a part of the optical slow-wave resonant intensity modulator [16]. In this modulator, a sampled grating is inscribed into the arms of a Mach–Zehnder GaAs–AlGaAs waveguide modulator, for which a delay factor of 2.9 has been achieved at 1543 nm. A sampled grating consists of a uniform grating with a length X and a spacer of a length S. The unit of a total length $X+S$ is repeated N times. At wavelengths within the stopband of a uniform Bragg grating, sampled gratings act as a cascaded Fabry–Perot resonator and reduce the group velocity of the light. Therefore, sampled gratings can enhance the modulation effect of the Mach–Zehnder modulator.

D. Progress in EIT-Based Slow Light

EIT refers to an artificially created spectral region of transparency in the middle of an absorption line due to the destructive quantum interference arising from two transitions in a three-level system [4], [5]. There are three basic energy level schemes for implementing a three-level EIT system interacting with two near-resonance electromagnetic fields (Fig. 4) [5]. In a ladder or cascade system, levels are arranged as E1 $<$ E2 $<$ E3; in a V scheme, levels are arranged as E2 $<$ E1 and E3; whereas in a Λ scheme, levels are arranged as E1, E3 $<$ E2. In all three cases, we label the transitions the same way: $|1\rangle$ to $|2\rangle$, and $|2\rangle$ to $|3\rangle$ are strong dipole-allowed transitions, while $|1\rangle$ to $|3\rangle$ is a dipole-forbidden transition. The signal field connecting $|1\rangle$ to $|2\rangle$ is the light field that one desires to slow down in a controllable fashion. The pump field is the control field connecting $|2\rangle$ to $|3\rangle$, whose intensity controls the amount of slowing down. In the literature, the pump laser is sometimes called the control laser.

As a result of the coherent coupling between the atomic system and the laser beams, atomic levels $|1\rangle$ and $|2\rangle$ are no longer eigenstates of the system. Instead, they are dressed by the pump laser and become two new states $|2\mathrm{d}\rangle$ and $|3\mathrm{d}\rangle$ (Fig. 5). This (destructive) quantum interference between two absorption paths produces a transparency spectral window in the middle of the strong $|1\rangle$ to $|2\rangle$ absorption line. The width of this transparency window is strongly dependent on the intensity of the pump light field.

By the Kramers–Kronig relations, the induced transparency, which is related to the imaginary part χ'' of the optical susceptibility χ, must be accompanied by a dispersive-shaped variation in the real part χ' of the susceptibility [Fig. 5(c)]. Such a variation leads to a very large positive derivative (or gradient) of the index of refraction $(n \equiv \mathrm{Re}\sqrt{1+\chi})$ with respect to frequency inside the center of the EIT transparency region. This slope results in a very large group index of refraction and, thus, a reduced group velocity [6]–[8].

The first demonstrations of ultraslow and stopped light pulses via EIT were accomplished using atomic vapors, both ultracold and at 80 °C, with impressive results [6], [7]. Slow-down factors as high as seven orders of magnitude have been demonstrated. Recently, slow and stopped light experiments was also achieved in a solid-state material, a praseodymium (Pr) doped Y_2SiO_5 (Pr : YSO) crystal [8].

The observed delay corresponds to a light group velocity of 33 m/s (70 mph) through the 3-mm-long crystal [8]. In defiance of theoretical estimates and conventional wisdom, the observed light pulse velocities are more than an order of magnitude slower than expected, based on the observed EIT linewidths. Although the reason for this is still being investigated, it is believed that it is because the ground state spin transition is inhomogeneously broadened, so that the ultimate light speed is not determined by this width, but rather by the much smaller homogeneous width. Stopped light was also demonstrated in this material. Observed storage times were up to 0.5 ms, which is the coherence time of the ground-state spin transition in the Pr ion. The experiments in Pr : YSO were performed at low temperatures, $\sim$5 K.

Several years ago, EIT-like signature was observed in intersubband coupled GaAs–AlGaAs quantum wells at a temperature as high as 30 K [17]–[19]. However, the observed EIT linewidth was considerably larger than desired due to effects such as interface roughness and many-body interactions. This occurred because the ground-state coherence involved states that were in different quantum wells of the coupled two-quantum-well system. There have been no slow-light experiments reported on semiconductor structures.

E. III-V QDs: Candidate for EIT-Based Slow Light in Semiconductor Structures

Semiconductor QDs have discrete electronic energy states due to three-dimensional (3-D) confinement. The discrete energy states make QDs an excellent candidate for slowing down light. Here, we review the state-of-the-art linewidth and uniformity properties that are important for obtaining slow light.

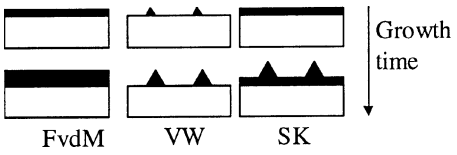

Fig. 6. Three growth modes for an as-grown epitaxy layer.

There have been many different approaches to make III-V QDs. Recently, there have been extensive research efforts on self-assembled (SA) growth of QDs on a single crystalline substrate. In general, the morphology of the as-grown epitaxy layer could evolve into three different modes without defects: layer-by-layer (Frank–van der Merwe or FvdM) growth mode, island growth (Volmer–Weber or VW) mode, and their combination, Stranski–Krastanow (SK) mode (Fig. 6). Different material system and growth conditions will determine different evolution routes [20]. In a lattice-matched system, the growth mode is governed solely by the interface and surface energies. If the sum of surface and interface energy is lower than the energy of the substrate surface, a uniform epitaxy layer is grown, and this is known as the FvdM mode. For a lattice-mismatched system with small interface energy, initial growth may occur layer by layer. However, as the layer is grown thicker, it has a larger strain energy and the as-grown layer tends to break into isolated islands to lower its total energy. This is the SK mode of growth.

Many experiments have shown that SK mode can form 3-D coherently strained islands under certain growth conditions. For a given shape, the elastic relaxation energy is proportional to the volume of the island. On the other hand, the elastic energy can also be relaxed in the form of dislocations. The interplay between the dislocation energy and the surface energy change due to island formation is determined by the amount of deposited material and growth condition. As the ratio between the dislocation energy and the surface energy change is large, i.e., the amount of surface energy change is appreciable during the island growth, the system favors the formation of coherent islands instead of dislocations. The positions of these dots are random and their size distribution as well as the density is determined by the growth condition including growth rate, chamber pressure, temperature, and growth interruption after dot material deposition. However, self-assembled growth allows vertical stacking of multiple QD layers to increase overall density.

SASK mode growth of QDs has been achieved in molecular beam epitaxy (MBE) [21], [22], metal–organic chemical vapor deposition (MOCVD) [23]–[25], and atomic layer epitaxy (ALE) [26]. Table 1 provides general comparisons. In MBE growth, the 2-D–3-D transition is monitored by reflective high-energy electron diffraction (RHEED), which leads to easier reproducibility and controllability. Due to high chamber pressure during growth in MOCVD, RHEED cannot be adopted as an *in situ* monitoring tool. On the other hand, MOCVD involves more chemical reactions such as metal–organic precursor cracking; therefore, the growth process is more toward a thermal equilibrium condition. Usually, QD growth requires low temperature, low chamber pressure, low growth rate, and a growth interruption phase. Nevertheless, MOCVD provides features such as different dot shape control, selective-area overgrowth, and atomic layer epitaxy, which cannot be easily achieved in a high-vacuum MBE environment.

Table 1
Comparison of QD Properties Using Three Growth Techniques

Epitaxy Method	MBE	MOCVD	MOCVD/ALE
Optical quality	Good	Good	Good
Dot density	$> 10^{11}/cm^2$	$> 10^{11}/cm^2$	$3x10^{10}/cm^2$
Linewidth	Good	Good	Excellent
Advantages	In-situ monitoring tool available; simpler to control	More choices on precursors; more possibilities for growth variations such as surface modification, patterned substrate and selective area epitaxy.	Same as MOCVD plus atomic layered control
Uniformity	30-60 meV	30-60 meV	20 meV
Typical dimensions	Lateral: 10-15nm Vertical: 2nm	Lateral: 10-15nm Vertical: 2nm	Lateral: 20 nm Vertical: 10 nm

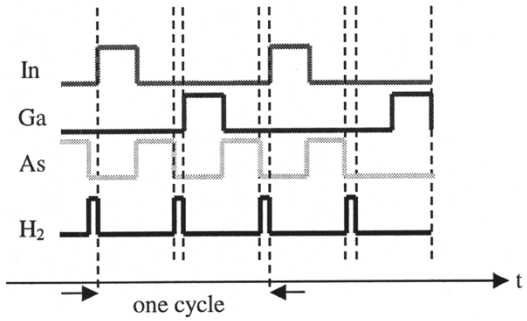

Fig. 7. Schematic of the source supply cycles for In, Ga, As, and hydrogen, respectively. The sequence of the supply in one cycle is In–As–Ga–As [27].

Atomic layer epitaxy (ALE) can be attained with slight modifications of the process for MOCVD self-assembled QD growth [26], [27]. The principle of ALE self-assembled growth is based on self-limited growth rate from metal–organic precursors under a low substrate temperature. Different sources are introduced to the substrate in an alternating fashion to achieve self-limited growth, as shown in Fig. 7. The QD formed by ALE has a shape closer to a sphere and, thus, has a larger thickness which results in a better electron confinement in the vertical direction. The role of alternate supply of sources leads to more uniform dots. The inhomogeneous linewidth of ALE grown QDs is thus the smallest of all techniques.

In the rest of the paper, we will analyze the slow-light performance in a semiconductor QD's structures. We will first prove the concept by hypothesizing a uniform QD array. We will then propose a new multicolor pump scheme to overcome the nonuniform problem in a realistic QD sample. Signal transmission simulation will be given in the end of the paper to demonstrate the feasibility of a QD-based optical buffer.

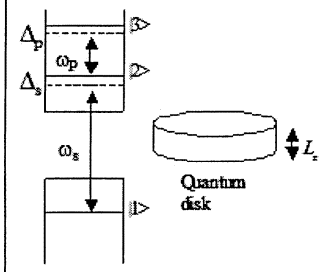

Parameters	Values
ω_S	1.36 μm
ω_P	12.8 μm
V	9 nm radius disk and 3.5 nm height
$\lvert\mu_{32}\rvert / e$	24.6 Å
$\lvert\mu_{21}\rvert / e$	21 Å
V / Γ	5×10^3 nm^3

Fig. 8. Quantum disk model used in our calculation. The table lists the relevant parameters.

II. Optical Buffer Design and QD Dipole Moment Calculations

There are many ways to physically construct the slow-light "active" region in semiconductor structures. We have chosen a simple three-level ladder scheme of InAs QD system where $|1\rangle$ is the first heavy hole band, and $|2\rangle$ and $|3\rangle$ are the first two electronic levels in the conduction band, as depicted in Fig. 8. Although this may not be an optimum system that will yield the largest slowdown factor, it is a better known system with the largest amount of characterization data available.

The material parameters listed here are calculated from effective-mass approximation for an InAs–GaAs QD system [2]. In this model, the dot is treated as a quantum disk with a radius a of 9 nm and a height h of 3.5 nm. Bandgap shifts due to the biaxial compressive strain are taken into account. The calculated transition wavelengths for the three-level system are 1.36 μm for C1 to HH1 transition and 12.8 μm for C2-C1 transition, respectively. The wave function of the quantum disk is obtained by solving the Schrödinger equation under the effective mass approximation. Each state can be characterized by three integral quantum numbers (mnl), where mn and l correspond to $\phi-\rho$ (transverse) and z dependence, respectively. The ranges for possible quantum numbers are as follows: $m \geq 0$, $l \geq 1$, and $n \geq 1$. The wave function of the state (mnl) at the position $r = (\rho, \phi, z)$ can be expressed as follows:

$$\phi_d(r) = C_{mn} \times \begin{cases} J_m(p\rho)\frac{e^{im\phi}}{\sqrt{2\pi}}\cos(k_z z) & \rho \leq a;\ |z| \leq \frac{h}{2} \\ J_m(p\rho)\frac{e^{im\phi}}{\sqrt{2\pi}}\cos\left(\frac{k_z h}{2}\right)e^{-\alpha\left(|z|-\frac{d}{2}\right)} & \rho \leq a;\ |z| > \frac{h}{2} \\ \frac{J_m(pa)}{K_m(qa)}K_m(q\rho)\frac{e^{im\phi}}{\sqrt{2\pi}}\cos(k_z z) & \rho > a;\ |z| \leq \frac{h}{2} \\ \frac{J_m(pa)}{K_m(qa)}K_m(q\rho)\frac{e^{im\phi}}{\sqrt{2\pi}}\cos\left(\frac{k_z d}{2}\right)e^{-\alpha\left(|z|\frac{d}{2}\right)} & \text{otherwise.} \end{cases} \quad (6)$$

In (6), $J_m(p\rho)$ and $K_m(q\rho)$ are the Bessel function of the first kind and the modified Bessel function of the second kind, respectively; C_{mn} is the wave function normalization constant; p, q, k_z, and α are constants to be determined from the boundary conditions at the interface between the quantum disk and the surrounding matrix [28].

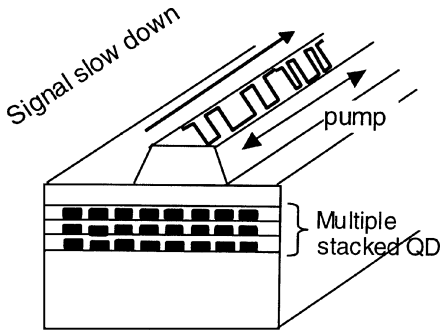

Fig. 9. Schematic of an optical buffer device based on semiconductor QD structures.

The intersubband dipole moment between the ground state (C1 or Level 2) and the first excited state (C2 or Level 3) of the conduction band is given by

$$\mu_{32} = \langle\phi_{d3}(r)|er|\phi_{d2}(r)\rangle\,. \quad (7)$$

On the other hand, the interband dipole moment can be expressed in terms of the momentum matrix element and the overlap integral of the wave functions $\phi_{d1}(r)$ and $\phi_{d2}(r)$ as follows [28].

$$\mu_{21} = \frac{e}{m_0\omega_{21}}\xi\,\langle u_c|\hat{p}|u_v\rangle\,\langle\phi_{d2}(r)|\phi_{d1}(r)\rangle \quad (8)$$

where $u_c(r)$ and $u_v(r)$ are periodic parts of the ground state for the electron and the hole, respectively. $\hat{p}$ is the momentum operator. ξ is an enhancement factor due to excitonic effects and its value is in the range of 41 to 949 [29]. In the GaAs–InAs–GaAs QD system described above, μ_{21} is calculated to be 20.4 eÅ, assuming $\xi = 4$. In the experiment, an interband dipole moment of 21 eÅ was reported in GaAs–AlGaAs QDs [30]. The calculated intersubband dipole moment in the transverse direction is 24.6 eÅ. As we will see later, a large μ_{21} and μ_{32} increases the slowdown factor.

As for the device structure, we chose a typical ridge waveguide configuration with multiple QD layers in its waveguide core layer. A schematic of the proposed buffer is given in Fig. 9. The signal and the pump optical beams copropagate or counterpropagate in the same waveguide. The pump light induces EIT and slows down the signal light velocity.

III. Slow-Light Analysis for Uniform QD System

A. Equations of Motion

To calculate the slowdown factor from (4) for a signal propagating in a uniform QD system, we need to know the refractive index change induced by the pump beam. For a three-level system shown in Fig. 8, the time-dependent optical dielectric constant ε experienced by the signal light can be derived from the semiclassical density-matrix ($\langle i|\hat{\rho}|j\rangle$) formulation.

Table 2
Measured Dephasing Times for Various Temperatures

Temperature (K)	T_2	$\hbar\gamma_H$	Reference
7	630ps	2 μeV	[31]
25	170ps	7.76 μeV	[31]
50	37ps	35.6 μeV	[31]
75	11ps	119.8 μeV	[31]
100	6ps	219.8 μeV	[31]
300	290±80fs	5.54meV (3.56 — 6.28 meV)	[32]

We define the slow-varying density matrices σ_{ij} in terms of the fully time-dependent $\langle i|\hat{\rho}|j\rangle$ as follows:

$$\begin{aligned}\langle 2|\hat{\rho}|1\rangle &= \sigma_{21}e^{-i\omega_s t}\\ \langle 3|\hat{\rho}|2\rangle &= \sigma_{32}e^{-i\omega_p t}\\ \langle 3|\hat{\rho}|1\rangle &= \sigma_{31}e^{-i(\omega_s+\omega_p)t}.\end{aligned} \tag{9}$$

The equations of motion for off-diagonal elements σ_{ij} of the density matrix are (rotating-wave approximation has been assumed) as follows:

$$\begin{aligned}\dot{\sigma}_{21} &= -(\gamma_{21}+i\Delta_s)\sigma_{21} - i\Omega_s(\rho_{22}-\rho_{11}) + i\Omega_p^*\sigma_{31}\\ \dot{\sigma}_{32} &= -(\gamma_{32}+i\Delta_p)\sigma_{32} - i\Omega_p(\rho_{33}-\rho_{22}) + i\Omega_s^*\sigma_{31}\\ \dot{\sigma}_{31} &= -(\gamma_{31}+i(\Delta_s+\Delta_p))\,\sigma_{31} + i\Omega_p\sigma_{21} - i\Omega_s\sigma_{32}.\end{aligned} \tag{10}$$

The equations of motion for the diagonal elements are as follows:

$$\begin{aligned}\dot{\rho}_{22} =& -\gamma_2\rho_{22} + (\Gamma_{3\to 2}\rho_{33} + \Gamma_{1\to 2}\rho_{11})\\ & - 2\mathrm{Im}\,(\Omega_s\sigma_{21}^* - \Omega_p\sigma_{32}^*)\\ \dot{\rho}_{32} =& -\gamma_3\rho_{33} + (\Gamma_{2\to 3}\rho_{22} + \Gamma_{1\to 3}\rho_{11}) - 2\mathrm{Im}\,(\Omega_p\sigma_{32}^*)\\ \dot{\rho}_{11} =& -(\dot{\rho}_{22}+\dot{\rho}_{33})\end{aligned} \tag{11}$$

where the Rabi frequency is $\Omega = \mu E/2\hbar$. $\Gamma_{i\to j}$ accounts for the population transfer rate from state $|i\rangle$ to $|j\rangle$. The signal and pump detuning are $\Delta_x \equiv \omega_{21}-\omega_S$ and $\Delta_p \equiv \omega_{32}-\omega_P$, respectively. The linewidths are defined as follows:

$$\begin{aligned}\gamma_i &= \sum_j \Gamma_{i\to j}\\ \gamma_{ij} &= \frac{1}{2}(\gamma_i+\gamma_j) + \gamma_{\mathrm{ph}}\end{aligned} \tag{12}$$

where γ_i and γ_{ph} are lifetime broadening and dephasing broadening linewidths, respectively. Usually, γ_{ph} is the dominant mechanism.

B. Dephasing Linewidths Versus Homogeneous Broadening Linewidths

In the density-matrix formula above, $\hbar\gamma$ ($\gamma = \gamma_{21}$ or γ_{31}) has the unit of energy and γ has the unit of angular frequency. In the literature, the full-width at half-maximum (FWHM) homogeneous broadening linewidth $\hbar\gamma_H$ (with a unit of energy) is related to the dephasing linewidths $\hbar\gamma$ through the following relationship (uncertainty principle):

$$\hbar\gamma_H = \frac{2\hbar}{T_2} \tag{13}$$

where $T_2 = 1/\gamma$ and we have assumed that the homogeneous broadening is dephasing dominated. Therefore

$$\hbar\gamma = \frac{\hbar\gamma_H}{2}. \tag{14}$$

Therefore, to convert T_2 into $\hbar\gamma$, we use

$$\hbar\gamma = \frac{\hbar}{T_2} = \frac{0.6591}{T_2(\mathrm{ps})}(\mathrm{meV}). \tag{15}$$

The measured dephasing time in InAs–GaAs QDs and the corresponding linewidth $\hbar\gamma$ are listed in Table 2 for various temperatures. Borri *et al.* [31] also measured the temperature dependence of $\hbar\gamma_H$, which translates to our dephasing linewidth to be

$$\hbar\gamma(T) = \hbar\gamma(T=300) - 0.01\times(300-T)\quad(\mathrm{meV}) \tag{16}$$

for temperature range $T = 125-300$ K.

C. Steady-State Solutions

At steady state, the solution to (10) gives the macroscopic dielectric constant around the signal frequency solution as follows:

$$\varepsilon_D(\omega\approx\omega_s) = \varepsilon_0\left[\varepsilon_{\mathrm{bac}} - i\frac{\Gamma|\mu_{21}|^2}{V\varepsilon_0}\frac{\eta_2}{\tilde{\gamma}_{21}\left(\frac{1+|\Omega_p|^2}{\tilde{\gamma}_{21}\tilde{\gamma}_{32}}\right)}\right] \tag{17}$$

where Γ is the optical confinement factor and V is the volume of a single QD. $\varepsilon_0 = 8.85\times 10^{-12}$ (F/m) and $\varepsilon_0\varepsilon_{\mathrm{bac}}$ is the background dielectric constant without coupling to any light. $\eta_2 = \rho_{22}-\rho_{11}$ is the population inversion for level $|2\rangle$. In (17), the complex detuning $\tilde{\gamma}_{31} = \gamma_{31} + i(\Delta_s+\Delta_P)$ and $\tilde{\gamma}_{21} = \gamma_{21} + i\Delta_s$ are defined. If EIT is reached, all the photo-created carriers are trapped in the ground state and the term η_2 has only contributions from thermally populated carriers. The group velocity reduction factor can be derived from the first derivative of the dielectric constant with respect to the frequency as follows:

$$S = n + \omega\frac{\partial n}{\partial\omega} = \mathrm{Re}\sqrt{\varepsilon} + \omega\frac{\partial \mathrm{Re}\sqrt{\varepsilon}}{\partial\omega}. \tag{18}$$

If both the signal and pump detuning vanish, the slowdown factor has an analytical form as follows:

$$\begin{aligned}S =& \left[\frac{\varepsilon_{\mathrm{bac}} + \sqrt{\varepsilon_{\mathrm{bac}}^2+\varepsilon_{\mathrm{res}}^2}}{2}\right]^{\frac{1}{2}}\\ & \times\left[1 + \frac{\hbar\omega_0}{2\sqrt{\varepsilon_{\mathrm{bac}}^2+\varepsilon_{\mathrm{res}}^2}}\frac{U_{21}\left(\Omega_{\mathrm{PP}}^2 - \tilde{\gamma}_{31}^2\right)}{\hbar^2\left(\tilde{\gamma}_{31}\tilde{\gamma}_{21}+\Omega_{\mathrm{PP}}^2\right)^2}\right]\end{aligned} \tag{19}$$

where

$$U_{21} = \Gamma|\mu_{21}|^2 \frac{(f_1 - f_2)}{V\varepsilon_0}$$

$$\Omega_{\rm PP}^2 = |\mu_{32}|^2 \frac{I_p}{4\hbar^2 c\varepsilon_0\sqrt{\varepsilon_{\rm bac}}}$$

$$\varepsilon_{\rm res}\left(\Omega_{\rm PP}^2\right) = \frac{U_{21}}{\hbar\left(\gamma_{21} + \frac{\Omega_{\rm PP}^2}{\gamma_{31}}\right)}. \tag{20}$$

In the above, $I_p = (c/\sqrt{\varepsilon_{\rm bac}})\varepsilon_0\varepsilon_{\rm bac}|E_p|^2$ is the pump power density (MW/cm^2); f_1 and f_2 are Fermi-Dirac occupation factors; the difference $f_2 - f_1$ is the steady-state value of the population inversion η_2. If the signal and pump detuning vanish, the absorption coefficient (in [1/cm]) experienced by the signal can be written as follows:

$$\alpha = \frac{\sqrt{2}\omega_S U_{21}}{\sqrt{\varepsilon_{\rm bac} + \sqrt{\varepsilon_{\rm bac}^2 + \varepsilon_{\rm res}^2}}\hbar c\left(\gamma_{21} + \frac{\Omega_{\rm PP}^2}{\gamma_{31}}\right)}. \tag{21}$$

The buffer has a storage time $\tau = LS\sqrt{\varepsilon_{\rm bac}}/c$ for a device of length L, and a turn-on threshold at pump power density $\Omega_{\rm PP,(min)}^2 = \gamma_{31}^2$. For a small $\varepsilon_{\rm res}$, S has a maximum when $\Omega_{\rm PP,(max)}^2 = \gamma_{31}(\gamma_{21} + 2\gamma_{31})$. For high pump power density and small γ_{31}, S approaches the upper bound of system performance proportional to

$$S_{\max} \propto \frac{1}{\gamma_{21}\gamma_{31}}. \tag{22}$$

Conversely, for low pump power density and large γ_{31}, we no longer have EIT, and the QD resumes a Lorentzian absorption spectrum.

D. Numerical Results

In Fig. 10, we plot the calculated imaginary and real part of the dimensionless dielectric constant $\varepsilon = \varepsilon_D/\varepsilon_0$ as a function of signal detuning Δ_s for uniform QD arrays with a 5.54-meV homogeneous broadening linewidth. The negative of the signal detuning is used to comply with the direction of signal frequency. As the pump power density is increased, the transparency window is widened. We can see that due to the finite linewidth of QDs, the absorption at signal wavelength ($\Delta_s = 0$) does not go to zero exactly. This is different from the EIT observed in atomic vapors. The absorption is reduced with a stronger pump.

The real part of ε in (b) follows the Kramers–Kronig relationship. The slope (derivative with respect to detuning) of this curve is proportional to the slowdown factor S, shown in Fig. 10(c). It is interesting to note that as the pump intensity increases, the maximum S value decreases, as also can be seen in the slope of curves in (b). However, it is constant over a larger range, proportional to the transparency window. It should be noted that for a high bit-rate signal with a large bandwidth, this constant slowdown regime needs to be optimized to minimize signal distortion and dispersion.

The slowdown factor S as a function of pump power density is shown in Fig. 11. Three different linewidth regimes are compared. Here, we assume $\hbar\gamma_{31} = \hbar\gamma_{21}$. The homogeneous linewidth $\hbar\gamma_H$ values of 2 μeV ($T = 7$ K), 0.1 meV ($T = 75$ K), and 5.54 meV ($T = 300$ K) were used for cases A, B, and C, respectively. Initially, as the pump power density increases, the slowdown factor increases. This is because as the two dressed states are formed, $\mathrm{d}\mathrm{Re}\varepsilon/\mathrm{d}\omega$ changes sign from negative to positive. As the power density continues to increase, the two dressed states are farther apart and the slowdown factor decreases, as clearly illustrated by Fig. 10. Hence, for a given linewidth, a maximum slowdown can be attained. The slowdown factors reach maximum values of 10^7, 3.4×10^4, and 51 at pump levels of 3×10^{-6}, 9×10^{-3}, and 2 MW/cm^2 for cases A, B, and C, respectively. This illustrates a strong dependence on the homogeneous linewidth. It is interesting to note that at higher pump density, say 100 MW/cm^2, the slowdown factor for all cases

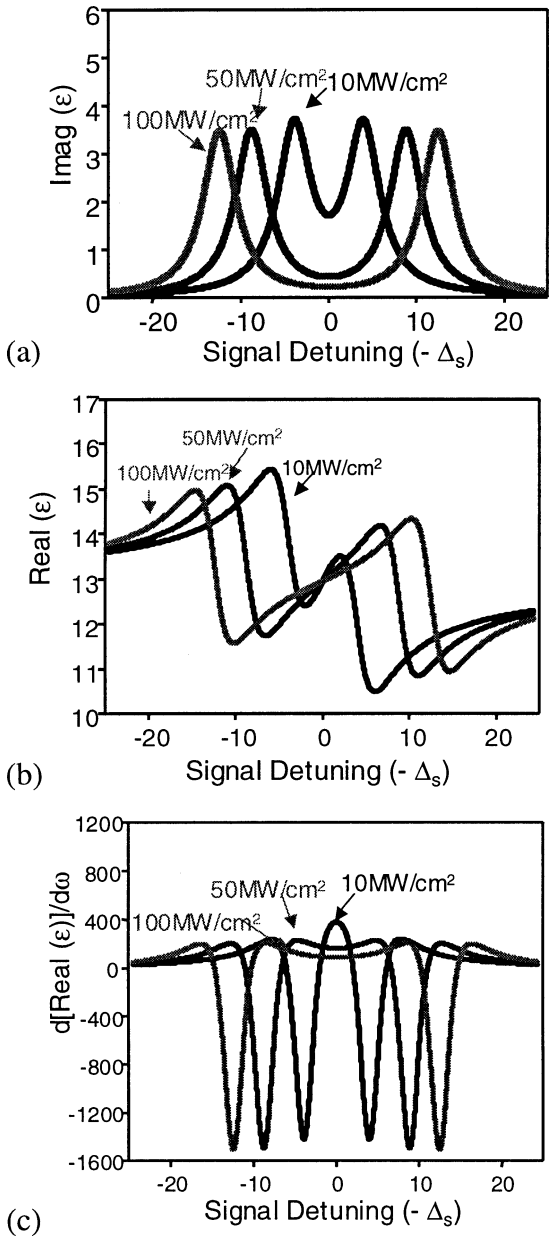

Fig. 10. Calculated (a) imaginary and (b) real part of dielectric constant, and (c) slope of real part of dielectric constant as a function of signal detuning Δ_S for uniform QD arrays with 5.54-meV homogeneous linewidths at various pump densities.

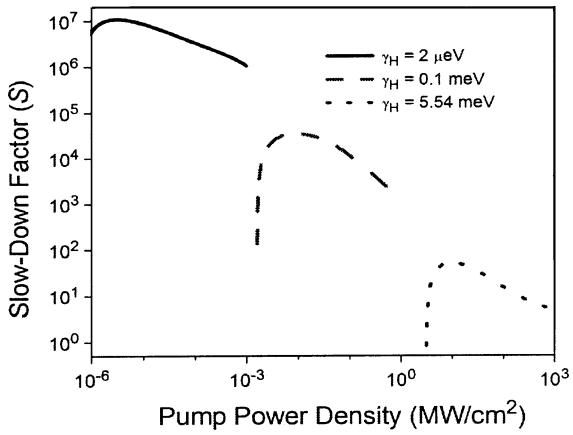

Fig. 11. Dependence of slowdown factor and the pump power density for different homogeneous linewidths.

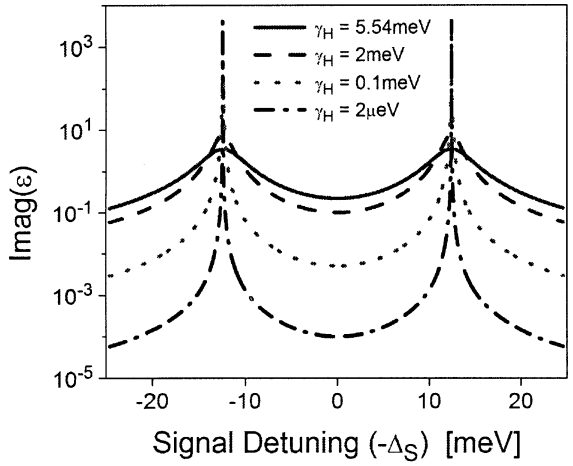

(a)

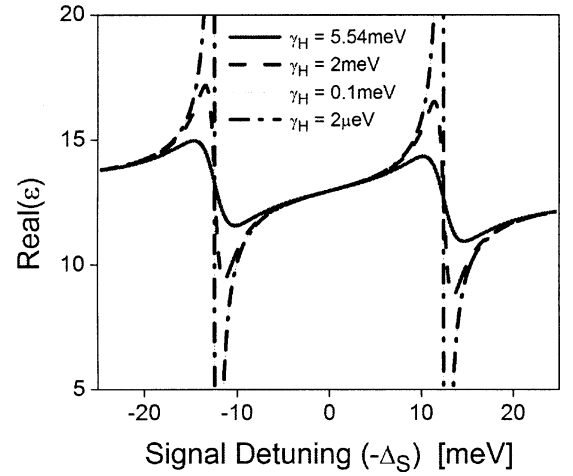

(b)

Fig. 12. Imaginary and real part of refractive index as a function of detuning energy for QDs with homogeneous linewidths of 2 μeV, 0.1, 2, and 5.54 meV under pump power density of 100 MW/cm^2.

approaching the same value. The imaginary and real part of refractive index for the three linewidths at 100 MW/cm^2 are shown in Fig. 12.

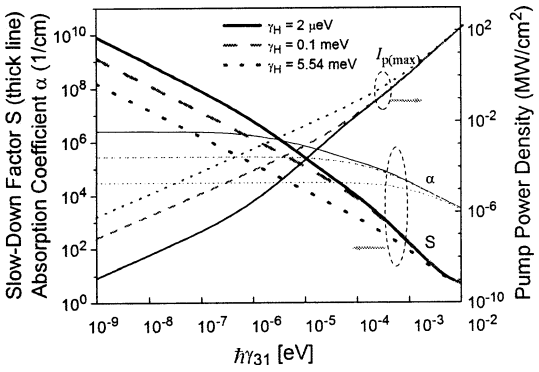

Fig. 13. Influence of $\hbar\gamma_{31}$ on slowdown factor, absorption coefficient, and required pump power density at three different homogeneous linewidth regimes. $\hbar\gamma_H$ are 2 μeV, 100 μeV, and 5.54 meV in cases A, B, and C, respectively.

Fig. 13 shows the influence of γ_{31}, if it could be independently controllable, on the slowdown factor, absorption coefficient, and pump power density. All are improved with the decrease of γ_{31}. Experimentally, a single QD has been shown to have μeV dephasing at low temperatures [31]. This would correspond to a slowdown factor of more than 10^7, requiring ~ 10 W/cm^2 pump power density. At room temperature, the dephasing linewidth $\hbar\gamma_{31}$ is 2.27 meV, attributed to phonon scattering, but a slowdown factor of 51 can still be achieved. The buffer turn-on and turn-off times depend on pump power density and are of the order of a few picoseconds (or less) for large (or small) linewidths with the above material parameters based on our transient model.

IV. Slow Light in a Nonuniform QD Array

A. Nonuniform QD Array

Experimentally, the PL measurement on a QD ensemble composed of many dots shows a linewidth of 20–60 meV, which is much larger than the homogeneous broadening linewidth. This linewidth is independent of temperature and is caused by nonuniform distribution of the dots. The nonuniformity comes from size, density, strain, and composition distributions.

The slow light in a QD array involves two laser sources, the signal and the pump, nearly in resonant with two excitonic states in QDs. Due to the nonuniformity of QDs, the signal and the pump will experience different detuning when interacting with different dots. Hence, the overall slowdown factor will be reduced. The signal wavelength is fixed by the application, and the signal detuning will be unavoidable for some of the QDs.

The dielectric constant experienced by a signal as given in (17) is a function of both signal and pump detuning. This is shown in Fig. 14, where the signal and pump detuning are adjusted separately. Since Δ_s appears twice in the denominator of (17) (Δ_s appears in both $\tilde{\gamma}_{21}$ and $\tilde{\gamma}_{32}$), the dependence on Δ_s is stronger. On the other hand, the slowdown factor also decreases with increasing pump detuning Δ_p.

It is perhaps easy to see that if one single wavelength pump source is used, the slowdown factor can be drastically

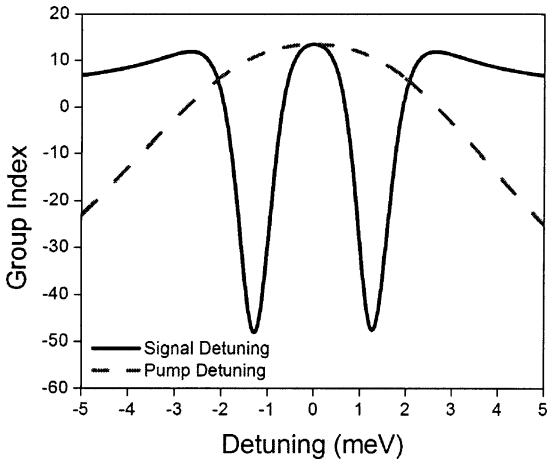

Fig. 14. Dependence of group index seen by the signal versus both the signal (Δ_s) and the pump (Δ_p) detuning. The signal detuning has more pronounced effects on the group index. In this plot, γ_{21} and γ_{31} are 1 meV. The pump power density is 2 MW/cm^2.

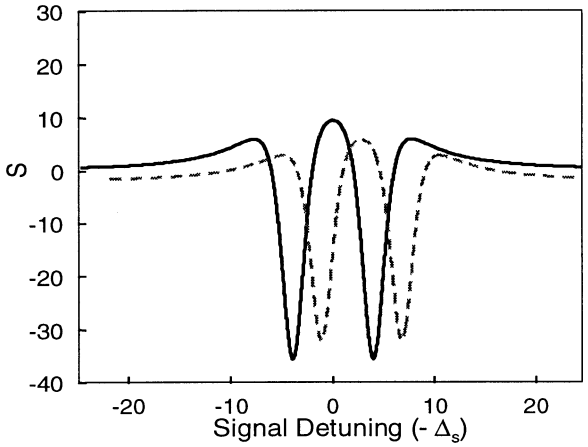

Fig. 15. Slowdown factor versus signal energy for two QD sizes with fixed signal and pump wavelengths aligned to one size. The dashed line is for the misaligned size.

reduced due to inhomogeneous broadening. In Fig. 15, we show the slowdown factor schematically for a case when there are two distinct QD sizes and the pump and signal wavelengths are aligned with only one. The slowdown factor for the misaligned case is shown by the dashed curve. As can be seen here, at the signal energy, the slowdown factor for the misaligned case can even be negative, hence cancelling the positive slowdown for the aligned QDs.

Given the above, we propose a multicolor pump scheme in which the pump is composed of many discrete frequency components. Each component will have different powers to optimize the performance. Schematically, with this new pumping scheme, Fig. 16 shows the slowdown factor for the same two-size QD case mentioned above. In this case, although the misaligned QDs would not contribute to a maximum slowdown, the degradation effect can be substantially reduced.

B. Model

The energy levels $|1\rangle$, $|2\rangle$, and $|3\rangle$ are the same as the ones used in Section II. In this section, however, particular attention is paid toward tracking the detuning values, as well as developing formula to track multiple pumps with different detuning. With the pump source composed of $2N+1$ multifrequency components $\omega_P^{(m)}(m=-N,\ldots,N)$, the equations of motion are similar to (10) and (11). For example, the equation for σ_{21} is now

$$\dot{\sigma}_{21} = -\tilde{\gamma}_{21}\sigma_{21} - i\Omega_S\eta_2 + i\sigma_{31}\sum_m \Omega_{Pm}^* e^{-i\left(\omega_P^{(n)}-\omega_P^{(m)}\right)t} \tag{23}$$

where $\Omega_{Pn} = \mu_{32}E_n/2\hbar$. The superscript (n) denotes the most resonant pump component to this particular group of QDs.

If we only keep the most resonant term in the summation, i.e., $m=n$ and neglect all the slowly varying exponential time factor, we obtain

$$\dot{\sigma}_{21} = -\tilde{\gamma}_{21}\sigma_{21} - i\Omega_S\eta_2 + i\sigma_{31}\Omega_{Pn}^*. \tag{24}$$

This approximation is valid if we consider steady-state solutions in which case only the longest time constant term will remain. To explicitly see this, we take Fourier transforms of (23) as follows:

$$\begin{aligned} -i\omega R_{21}(\omega) = &-\tilde{\gamma}_{21}R_{21}(\omega) + i\Omega_S\left(R_{11}(\omega) - R_{22}(\omega)\right) \\ &+ i\sum_m \Omega_{Pm}^* R_{31}\left(\omega - \omega_P^{(m)}\right) \end{aligned} \tag{25}$$

where R_{21} is the Fourier transform of the corresponding slowly varying density matrix σ_{21}. At steady state, only zero-frequency component contributes, that is, only $R_{21}(0)$ will contribute provided the other components are far away compared with the dephasing linewidth γ_{21}. If the spacing between two adjacent pump components is less than γ_{21}, a full set of coupled nonlinear differential equations have to be solved and is under investigation. On the other hand, if the spacing between two adjacent pump components is larger than γ_{21}, (25) becomes

$$0 = -\tilde{\gamma}_{21}R_{21}(0) + i\Omega_S\left(R_{11}(0) - R_{22}(0)\right) + i\Omega_{Pn}^* R_{31}(0). \tag{26}$$

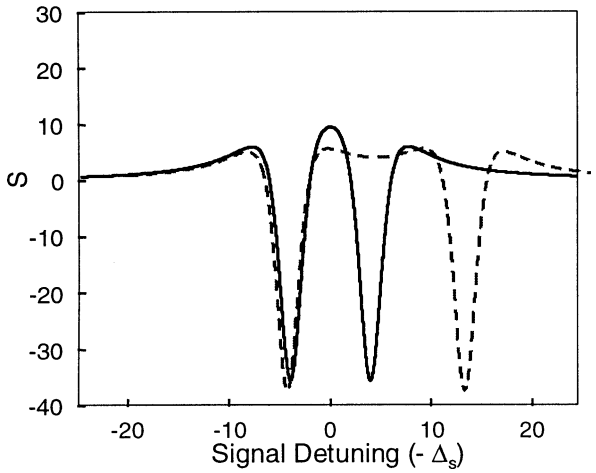

Fig. 16. Slowdown factor versus signal energy for two QD sizes with fixed signal and two pump wavelengths having different pump powers. The dashed line is for the misaligned size.

This justifies that the nonresonant terms at steady state do not contribute.

The probability that a QD group has energy level deviate from the central value (denoted by superscript 0) is assumed to satisfy the Gaussian distribution as follows:

$$\Pr\left(\omega_{21}=\omega_{21}^{(0)}+\delta\omega_{21}\right)=\frac{1}{\sqrt{\pi}\Gamma_{\rm inh}}\exp\left(-\frac{\delta\omega_{21}^2}{\Gamma_{\rm inh}^2}\right) \quad (27)$$

where $\Gamma_{\rm inh}=0.6\hbar\gamma_{\rm inh}$ in which $\hbar\gamma_{\rm inh}$ is the FWHM inhomogeneous broadening linewidth.

C. Steady-State Dielectric Constant for a Nonuniform QD Array

The solution at steady state is very similar to it as in Section III, except now we have to carry out the explicit index label of a particular QD group. We assume EIT is reached and all the photo-created carriers will be trapped in the ground state, that is, $\eta_2\approx -1$. The (dimensionless) macroscopic dielectric constant experienced by the signal field is given by

$$\varepsilon\approx\varepsilon_{\rm bac}+\int {\rm d}\delta\omega_{21}\frac{\frac{iU_{21}}{\hbar}}{(\gamma_{21}+i\delta\omega_{21})+\frac{\Omega_{\rm PP}^{(n)2}}{\left(\gamma_{31}+i\left(\delta\omega_{21}+\Delta_P^{(n)}\right)\right)}} \quad (28)$$

where

$$\begin{aligned}\Delta_P^{(n)}&=\omega_{32}^{(0)}+\delta\omega_{32}-\omega_P^{(n)}\\ U_{21}&\simeq\Pr\left(\omega_{21}^{(0)}\right)\frac{\Gamma}{V}|\mu_{21}|^2\frac{(f_1-f_2)}{\varepsilon_0}\\ \Omega_{\rm PP}^{(n)2}&=\frac{|\mu_{32}|^2I_P^{(n)}}{4\hbar^2c\varepsilon_0\sqrt{\varepsilon_{\rm bac}}}\end{aligned} \quad (29)$$

f_1-f_2 is the steady state value of the average population inversion between level 1 and 2 thermally populated (we have excluded the photo-created carriers by assuming EIT). We have assumed the dipole moments are identical for all QD groups.

D. Multicolor Pumping Scheme

Consider a multiple-color pump source with discrete spacing as shown in Fig. 17. Each component is allowed to have different power. Consider a 20-meV inhomogeneous linewidth (also plotted in Fig. 17 for comparison) and two cases of homogeneous broadening linewidth ($\hbar\gamma_H$) of 5.54 meV (room temperature value) and 2 meV. Let $V^{(0)}/\Gamma^{(0)}=5\times10^3$ nm^3 in the simulation. The interband μ_{21} and intersubband dipole moments are the same values used in Fig. 8.

Fig. 18 shows the slowdown factor versus pump power density for a nonuniform QD with a single pump as compared against a uniform QD array. The single pump is aligned with the average energy separation between $|2\rangle$ and $|3\rangle$. Significant degradation of slowdown factor was obtained. The maximum slowdown factors are 244 and 51.4 for 2 and 5.54 meV $\hbar\gamma_H$, respectively, for a uniform QD array. Whereas for the

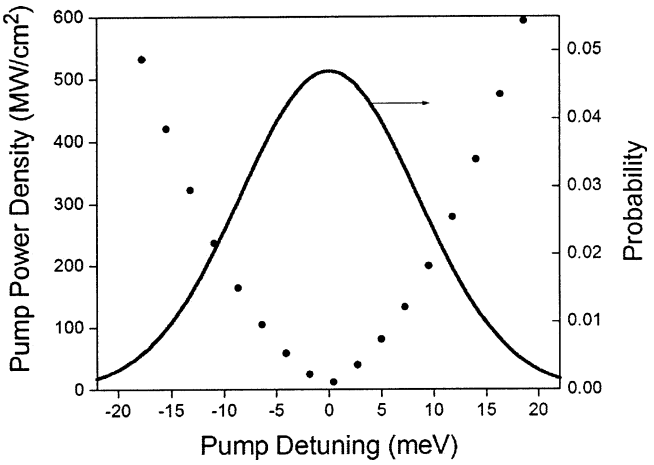

Fig. 17. Pump power density for each pump components at different detuning. The spacing between two adjacent pump components is 2.27 meV in this plot. The blue Gaussian curve shows the probability of finding a particular group of QD with energy levels deviated from the average value of the whole ensemble by the amount determined from the x axis.

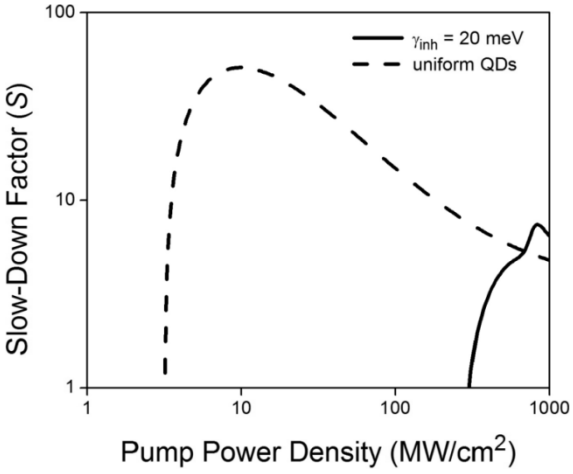

Fig. 18. Slowdown factor as a function of pump density for a single pump scheme. The QD medium has a homogeneous linewidth of 5.54 meV and inhomogeneous linewidth of 20 meV due to QD nonuniformity. The case of uniform QDs is also shown for comparison (dashed line).

case with 20 meV nonuniformity and a single pump source, the maximum slowdown factors were reduced to ∼40 and ∼10, respectively.

On the other hand, if a multicolor pump source is used, the degradation can be greatly improved. Fig. 19 shows the slowdown factor degradation for a variety of pump component spacing, normalized to the homogeneous broadening linewidth $\hbar\gamma_H$. The slowdown factor degradation is defined as the ratio between the slowdown factors in QD arrays with and without nonuniformity. In the calculation, we looked for a scheme to achieve the highest slowdown factor. A denser pump array has less degradation. The dashed line represents the case the pump spacing and the homogeneous linewidth are equal. The maximum slowdown factors could be still ∼40 for 5.54 meV $\hbar\gamma_H$ with 20 meV inhomogeneous broadening.

Fig. 17 shows the optimized pump power density for each pump component for the case that homogeneous linewidth

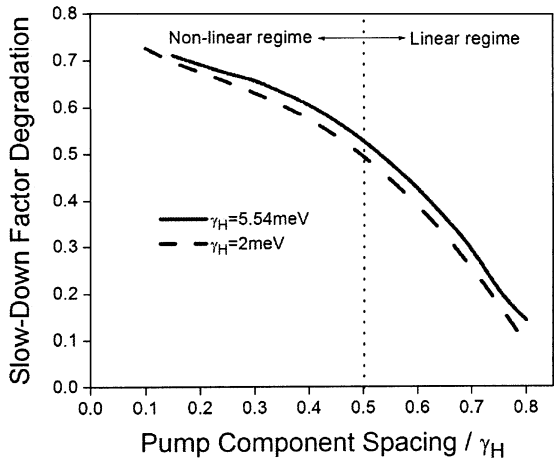

Fig. 19. Slowdown factor degradation due to QD nonuniformity.

is 5.54 meV and the spacing between two pump components is 2.27 meV. In the results above, the pump components are equally spaced in frequency. The more general case that the pump components are not equally spaced is under investigation.

V. Signal Propagation Through QD-Based Optical Buffers

In this section, we show the effect of signal propagation through a QD-based optical buffer discussed in Section III. Here, for simplicity sake, we consider only uniform QDs. We believe the nonuniformity factor can be treated simply with a slowdown reduction factor, similar to what was described in Section IV.

In frequency domain, the output of the buffer can be related to the input signal via a system transfer function $H(\omega)$ given by

$$H(\omega) = e^{ik_z L} \tag{30}$$

where L is the length of the buffer and k_z, the propagation constant in the z (waveguide) direction, is related to the dielectric constant by

$$k_z^2(\omega) = \frac{\omega^2}{c^2}\varepsilon(\omega). \tag{31}$$

For a given set of material parameters including the pump power density, we can calculate k_z and, thus, the transfer function $H(\omega)$. The output signal is simply the inverse Fourier transform of the product of the input signal and $H(\omega)$.

The input signal is a Gaussian pulse train with a repetition rate of 10 Gb/s and pulse FWHM 100 ps. We set the homogeneous broadening linewidth to be 2 meV and used InAs–GaAs QDs with material parameters given in Fig. 8. The pump power density is fixed at 2 MW/cm^2, which corresponds to the maximum slowdown factor $\sim$244. The output signal has a larger FWHM due to the nonflat frequency response. The result is shown in Fig. 20(a). The FWHM increases as the device length increases and becomes 104 ps when L is 1 cm. Fig. 20(b) shows the dependence of the total buffering capacity with the pump power density. The buffer

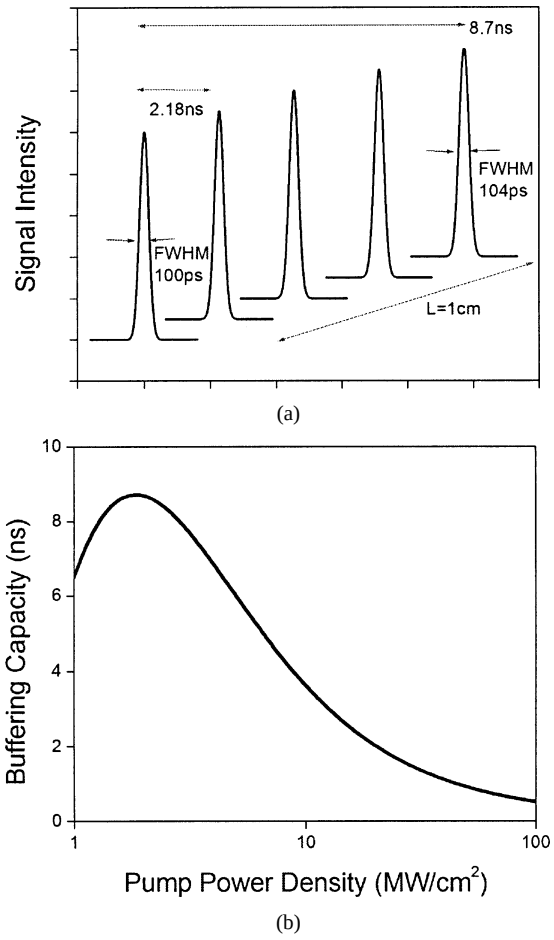

Fig. 20. (a) Signal propagation through a QD waveguide with the length of 1 cm. (b) Control of the slowdown factor with the pump power density.

capacity can be externally controlled via the change of the pump power. The control is continuous and can vary from 1 bit up to 87 bits [3].

VI. Conclusion

We proposed and analyzed the first semiconductor all-optical buffer based on EIT effect in QDs. We establish the conditions and formulation necessary to achieve a large slowdown factor. The light pulses can slow down significantly with a negligible dispersion, making it desirable for making optical buffers with an adjustable storage. The effect of QD size nonuniformity is also calculated. Although the linewidth of QDs is found to be critical, our calculations show that a slowdown factor of $\sim$40 can be obtained with state-of-the-art QDs at room temperature using a novel multiple pump scheme. Our theoretical model shows that a buffering time of 8.7 ns in a 10-Gb/s system could be obtained at room temperature without pulse distortion and spreading for a uniform QD waveguide. This level of storage is already interesting for a number of applications. With the improvements of QD linewidth and uniformity in the future, the slowdown and storage can no doubt increase to a larger number, making them far more useful. We also anticipate that further optimization in device design and energy

configuration can lead to significantly increased slowdown factor. We believe an optical buffer would serve as a critical catalyst to trigger new architectures and applications in optical networks, communications, and signal processing.

REFERENCES

[1] P. C. Ku, C. J. Chang-Hasnain, and S. L. Chuang, "Variable semiconductor all-optical buffers," *Electron. Lett.*, vol. 38, pp. 1581–1583, Nov. 2002.

[2] J. Kim, S. L. Chuang, P. C. Ku, and C. J. Chang-Hasnain, "Slow-light in a variable semiconductor all-optical buffer using quantum dots," *Appl. Phys. Lett.*, submitted for publication.

[3] P. C. Ku, C. J. Chang-Hasnain, J. Kim, and S. L. Chuang, "Semiconductor all-optical buffers using quantum dots in resonator structures," in *Proc. OFC'03*, Atlanta, GA, Mar. 2003.

[4] S. E. Harris, "Electromagnetically induced transparency," *Phys. Today*, vol. 50, pp. 36–42, July 1997.

[5] J. P. Marangos, "Electromagnetically induced transparency," *J. Modern Opt.*, vol. 45, pp. 471–503, Mar. 1998.

[6] L. V. Hau, S. E. Harris, Z. Dutton, and C. H. Behroozi, "Light speed reduction to 17 meters per second in an ultracold atomic gas," *Nature*, vol. 397, pp. 594–598, Feb. 1999.

[7] D. F. Phillips, A. Fleischhauer, A. Mair, R. L. Walsworth, and M. D. Lukin, "Storage of light in atomic vapor," *Phys. Rev. Lett.*, vol. 86, pp. 783–786, Jan. 2001.

[8] A. V. Turukhin, V. S. Sudarshanam, M. S. Shahriar, J. A. Musser, B. S. Ham, and P. R. Hemmer, "Observation of ultraslow and stored light pulses in a solid," *Phys. Rev. Lett.*, vol. 88, p. 023 602, Jan. 2002.

[9] *J. Lightwave Technol. (Special Issue on Optical Networks)*, vol. 18, Dec. 2000.

[10] A. Molony, L. Zhang, J. A. R. Williams, I. Bennion, C. Edge, and J. Fells, "Fiber Bragg-grating true time-delay systems: discrete-grating array 3-b delay lines and chirped-grating 6-b delay lines," *IEEE Trans. Microwave Theory Tech.*, vol. 45, pp. 1527–1530, Aug. 1997.

[11] J. L. Corral, J. Martí, S. Regidor, J. M. Fuster, R. Laming, and M. J. Cole, "Continuously variable true time-delay optical feeder for phased-array antenna employing chirped fiber grating," *IEEE Trans. Microwave Theory Tech.*, vol. 45, pp. 1531–1536, Aug. 1997.

[12] G. Lenz, B. J. Eggleton, C. K. Madsen, and R. E. Slusher, "Optical delay lines based on optical filters," *IEEE J. Quantum Electron.*, vol. 37, pp. 525–532, Apr. 2001.

[13] R. Langenhorst, M. Eiselt, W. Pieper, G. Grosskopf, R. Ludwig, L. Kuller, E. Dietrich, and H. G. Weber, "Fiber loop optical buffer," *J. Lightwave Technol.*, vol. 14, pp. 324–335, Mar. 1996.

[14] K. O. Hill and G. Meltz, "Fiber Bragg grating technology fundamentals and overview," *J. Lightwave Technol.*, vol. 15, pp. 1263–1276, Aug. 1997.

[15] J. B. Khurgin, "Light slowing down in Moire fiber gratings and its implications for nonlinear optics," *Phys. Rev. A, Gen. Phys.*, vol. 62, p. 013 821, July 2000.

[16] N. Show, W. J. Stewart, J. Heaton, and D. R. Wight, "Optical slow-wave resonant modulation in electro-optic GaAs/AlGaAs modulators," *Electron. Lett.*, vol. 35, pp. 1557–1558, Sept. 1999.

[17] J. Faist, F. Capasso, C. Sirtori, K. W. West, and L. N. Pfeiffer, "Controlling the sign of quantum interference by tunneling from quantum wells," *Nature*, vol. 390, pp. 589–591, Dec. 1997.

[18] C. C. Phillips, E. Paspalakis, G. B. Serapiglia, C. Sirtori, and K. L. Vodopyanov, "Observation of electromagnetically induced transparency and measurements of subband dynamics in a semiconductor quantum well," *Physica E*, vol. 7, pp. 166–173, Apr. 2000.

[19] H. Schmidt, K. L. Campman, A. C. Gossard, and A. Imamoglu, "Tunneling induced transparency: Fano interference in intersubband transitions," *Appl. Phys. Lett.*, vol. 70, pp. 3455–3457, June 1997.

[20] D. Bimberg, M. Grundmann, and N. N. Ledentsov, *Quantum Dot Heterostructures*. New York: Wiley, 1999, ch. 3.

[21] D. Bimberg, M. Grundmann, N. N. Ledentsov, S. S. Ruvimov, P. Werner, U. Richter, J. Heydenreich, V. M. Ustinov, P. S. Kop'ev,, and Z. I.Zh. I. Alferov, "Self-organization processes in MBE-grown quantum dot structures," *Thin Solid Films*, vol. 267, pp. 32–36, Oct. 1995.

[22] J. M. Moison, F. Houzay, F. Barthe, L. Leprince, E. André, and O. Vatel, "Self-organized growth of regular nanometer-scale InAs dots on GaAs," *Appl. Phys. Lett.*, vol. 64, pp. 196–198, Jan. 1994.

[23] F. Heinrichsdorff, A. Krost, M. Grundmann, D. Bimberg, A. O. Kosogov, and P. Werner, "Self-organization processes of InGaAs/GaAs quantum dots grown by metalorganic chemical vapor deposition," *Appl. Phys. Lett.*, vol. 68, pp. 3284–3286, June 1996.

[24] N. N. Ledentsov, J. Böhrer, D. Bimberg, I. V. Kochnev, M. V. Maximov, P. S. Kop'ev, Z. I.Zh. I. Alferov, A. O. Kosogov, S. S. Ruvimov, P. Werner, and U. Gösele, "Formation of coherent superdots using metal-organic chemical vapor deposition," *Appl. Phys. Lett.*, vol. 69, pp. 1095–1097, Aug. 1996.

[25] F. Heinrichsdorff, M. H. Mao, N. Kirstaedter, A. Krost, D. Bimberg, A. O. Kosogov, and P. Werner, "Room-temperature continuous-wave lasing from stacked InAs/GaAs quantum dots grown by metalorganic chemical vapor deposition," *Appl. Phys. Lett.*, vol. 71, pp. 22–24, July 1997.

[26] K. Mukai, N. Ohtsuka, H. Shoji, and M. Sugawara, "Growth and optical evaluation of InGaAs/GaAs quantum dots self-formed during alternate supply of precursors," *Appl. Surf. Sci.*, vol. 112, pp. 102–109, Mar. 1997.

[27] K. Mukai, M. Sugawara, M. Egawa, and N. Ohtsuka, "Metalorganic vapor phase epitaxial growth of self-assembled InGaAs/GaAs quantum dots," in *Self-Assembled InGaAs/GaAs Quantum Dots*, M. Sugawara, Ed. San Diego, CA: Academic, 1999, vol. 60, Semiconductors and Semimetals, pp. 155–181.

[28] S. L. Chuang, *Physics of Optoelectronic Devices*. New York: Wiley, 1995.

[29] T. Kataoka, T. Tokizaki, and A. Nakamura, "Mesoscopic enhancement of optical nonlinearity in CuCl quantum dots: giant-oscillator-strength effect on confined excitons," *Phys. Rev. B, Condens. Matter*, vol. 48, pp. 2815–2818, July 1993.

[30] J. R. Guest, T. H. Stievater, X. Li, J. Cheng, D. G. Steel, D. Gammon, D. S. Katzer, D. Park, C. Ell, A. Thränhardt, G. Khitrova, and H. M. Gibbs, "Measurement of optical absorption by a single quantum dot exciton," *Phys. Rev. B, Condens. Matter*, vol. 65, p. 241 310, June 2002.

[31] P. Borri, W. Langbein, S. Schneider, U. Woggon, R. L. Sellin, D. Ouyang, and D. Bimberg, "Ultralong dephasing time in InGaAs quantum dots," *Phys. Rev. Lett.*, vol. 87, p. 157 401, Oct. 2001.

[32] P. Borri, W. Langbein, J. Mørk, J. M. Hvam, F. Heinrichsdorff, M. H. Mao, and D. Bimberg, "Dephasing in InAs GaAs quantum dots," *Phys. Rev. B, Condens. Matter*, vol. 60, pp. 7784–7787, June 1999.

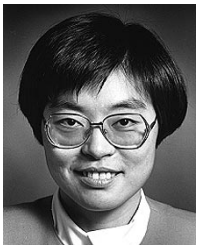

Connie J. Chang-Hasnain (Fellow, IEEE) received the B.S. degree from the University of California, Davis, and the M.S. and Ph.D. degrees from the University of California, Berkeley, all in electrical engineering, in 1982, 1984, and 1987, respectively.

She was a Member of Technical Staff at Bellcore from 1987 to 1992. From April 1992 to December 1995, she was Associate Professor of Electrical Engineering at Stanford University, Stanford, CA. Since January 1996, she has been Professor of Electrical Engineering at the University of California, Berkeley. She founded BANDWIDTH9 Inc. in 1997 and served as its Chairman, President, and CEO from 1997 to 2000. She has authored more than 200 papers in leading technical journals and conferences, six book chapters, and presented over 100 invited talks. She was also awarded 18 patents. Her research interest has been in the area of semiconductor optoelectronic devices, with a particular focus on wavelength-engineered vertical cavity lasers and detectors, and novel systems applications.

Prof. Chang-Hasnain is a Presidential Faculty Fellow, Packard Fellow, Alfred P. Sloan Research Fellow, and National Young Investigator. She was named the Outstanding Young Electrical Engineer by Eta Kappa Nu in 1992. She received the 1994 Distinguished Lecturer Award of IEEE Lasers and Electro-Optics Society and the 1999 Curtis W. McGraw Research Award from the American Society of Engineering Education. She served as General Chair of 1999 Conference on Lasers and Electro-Optics (CLEO) and 1997 Conference Chair of the first VCSEL Conference. She was an editor of the *IEEE Circuits and Devices Magazine* and 1998 Guest Editor of IEEE JOURNAL OF SELECTED TOPICS IN QUANTUM ELECTRONICS Special Issue on Semiconductor Lasers. She was a LEOS Board of Governor from 1992 to 1995 and is a current Board of Director of the Optical Society of America (OSA). She was a member of the U.S. Air Force Scientific Advisory Board from 1997 to 1999. She is a Fellow of the OSA.

Pei-Cheng Ku (Student Member, IEEE) was born in Taipei, Taiwan, R.O.C., in 1973. He received the B.S. degree in electrical engineering from the National Taiwan University, Taipei, in 1995. He is currently working toward the Ph.D. degree in the Department of Electrical Engineering and Computer Science, University of California, Berkeley, under the Berkeley Fellowship.

He was a research and teaching assistant at National Taiwan University from 1995 to 1996. He served in the Taiwan Navy from 1996 to 1998 as an Ensign Instructor and Engineering Officer at the Naval Technical School. His research interests include optoelectronic materials and devices, nanostructures, biophotonics, and theoretical physics.

Mr. Ku was elected as an honorary member of Phi-Tau-Phi in 1995.

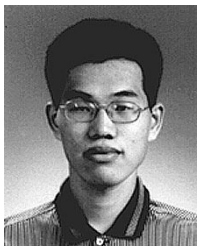

Jungho Kim received the B.S. and M.S. degrees in electrical engineering from Seoul National University, Seoul, Korea, in 1998 and 2000, respectively. He is currently working toward the Ph.D. degree in the Department of Electrical and Computer Engineering, University of Illinois at Urbana-Champaign, Urbana. In 2000, his M.S. thesis was selected as one of the distinguished M.S. theses from the School of the Electrical Engineering, Seoul National University.

From 2000 to 2001, he was a full-time Member of Research Staff at the Electrical Engineering and Science Research Institute, Seoul, Korea. His research interests are physics of quantum optics and optoelectronic devices, especially in quantum-dot and quantum-well systems. He is also interested in bidirectional optical transmission systems, applications of a fiber Bragg grating, and Monte Carlo simulation.

Mr. Kim won a silver prize in the 6th Human Tech Thesis Contest sponsored by Samsung Electronics.

Shun-Lien Chuang (Fellow, IEEE) received the B.S. degree in electrical engineering from National Taiwan University, Taipei, Taiwan, R.O.C., in 1976, and the M.S., E.E., and Ph.D. degrees in electrical engineering from the Massachusetts Institute of Technology, Cambridge, in 1980, 1981, and 1983, respectively.

In 1983, he joined the Department of Electrical and Computer Engineering at the University of Illinois at Urbana-Champaign, Urbana, where he is currently a Professor and Director of the Illinois Program for Photonics and Optoelectronics. He was a Resident Visitor at AT&T Bell Laboratories, Murray Hill, NJ, in 1989; a Senior Visiting Professor (Sabbatical Chair) at the SONY Research Center in 1995; and an Invited Professor at NTT Basic Research Laboratories in 1997. He was also a visitor at NASA Ames Research Center in the summer of 1999, and at Fujitsu Research Laboratories in the summer of 2000. He was on sabbatical leave as a Visiting Professor (EPSRC Fellow) at Cavendish Laboratory, University of Cambridge, Cambridge, U.K., in 2002. He is conducting research on strained quantum-well and quantum-dot semiconductor lasers, modulators, infrared detectors, fiber optic sensors, and optical networks. He is leading a multidisciplinary university research initiative (MURI) team conducting research on fundamental issues of infrared photodetectors and a NSF-ITR group project on high-speed wavelength agile optical networks. He is the author of *Physics of Optoelectronic Devices* (New York: Wiley, 1995). He has published more than 240 journal and conference papers and has given many invited talks at conferences and institutions.

He was an Associate Editor of the IEEE JOURNAL OF QUANTUM ELECTRONICS (1997–2003). He was a Feature Editor for the *Journal of Optical Society of America B*, Special Issue on Terahertz Generation, Physics and Applications in 1994. He also edited a feature section on Mid-Infrared Quantum-Cascade Lasers in the June 2002 issue of the JOURNAL OF QUANTUM ELECTRONICS. He is a Fellow of the Optical Society of America, and a member of the American Physical Society. He has been cited many times for Excellence in Teaching at the University of Illinois. He received the Andersen Consulting Award for excellence in advising in 1994 and was selected as an Associate at the Center for Advanced Study at the University of Illinois in 1995. He was also awarded a Fellowship from the Japan Society for the Promotion of Science to visit the University of Tokyo in 1996.